energies

MDPI

Article

Hybrid Anionic Electrolytes for the High Performance of Aqueous Zinc-Ion Hybrid Supercapacitors

Bin Xie [1], Junjie He [1,2,3,*], Yuchen Sun [2], Senlin Li [2] and Jing Li [2,3,*]

[1] Biomass New Materials Research Center, College of Architectural Engineering, Yunnan Agricultural University, Kunming 650201, China
[2] Department of Science and Technology, Yunnan Agricultural University, Kunming 650201, China
[3] Yunnan International Joint R&D Center of Smart Agriculture and Water Security, Yunnan Agricultural University, Kunming 650201, China
* Correspondence: junjiehe@ynau.edu.cn (J.H.); li_jing69@ynau.edu.cn (J.L.); Tel.: +86-133-0885-9685 (J.H.)

Abstract: Aqueous zinc-ion hybrid supercapacitors (AZHSs) are promising candidates for powering mobile devices due to their intrinsically high safety, the high theoretical capacity of zinc anodes, and the wide range of sources of raw materials for activated carbon (AC) cathodes. Here, we report that there is a synergistic effect between the anions of an AZHS electrolyte, which can significantly improve the specific capacity and rate capability of an AC cathode. The results showed that the specific capacities of the AC cathode//2 M $ZnSO_4$(aq)//Zn anode energy storage system were 115 and 41 mAh g^{-1} at 0.1 and 5 A g^{-1} current densities, respectively. The specific capacity at a 0.1 A g^{-1} current density was enhanced to 136 mAh g^{-1} by doping 0.5% $ZnCl_2$ and 0.5% $Zn(CF_3SO_3)_2$ in the 2 M $ZnSO_4$ electrolyte. The specific capacity at a 5 Ag^{-1} current density was enhanced to 69 mAh g^{-1} by doping 1% $ZnCl_2$ and 0.5% $Zn(CF_3SO_3)_2$ in the 2 M $ZnSO_4$ electrolyte. In addition, the co-doped electrolyte increased the energy consumption of the binding of the AC surface groups with H^+ and inhibited the precipitation of $Zn_4SO_4(OH)_6{\cdot}5H_2O$. This provides an important perspective for improving the performance of AZHSs.

Keywords: aqueous zinc-ion hybrid supercapacitors; electrolyte; energy storage; co-doped

Citation: Xie, B.; He, J.; Sun, Y.; Li, S.; Li, J. Hybrid Anionic Electrolytes for the High Performance of Aqueous Zinc-Ion Hybrid Supercapacitors. *Energies* **2023**, *16*, 248. https://doi.org/10.3390/en16010248

Academic Editor: James M. Gardner

Received: 5 December 2022
Revised: 16 December 2022
Accepted: 21 December 2022
Published: 26 December 2022

1. Introduction

The commitment of countries to solve the problem of global warming has led to a boom in research and practice on carbon emission mitigation, especially in the promotion and application of electric vehicles and electric agricultural machinery that replace oil-fired combustion with electricity [1–3]. The most critical technology for these electricity-powered mechanical devices is the energy storage system [4–6], so there is an urgent requirement to develop high-performance, safe, and inexpensive energy storage devices. Aqueous zinc-ion hybrid supercapacitors (AZHSs) inherit the high-power function of supercapacitors (SCs) and many advantages of some batteries [7] and have become one of the most promising candidates for promoting the application of electric vehicles and electric agricultural machinery. The zinc anodes of AZHSs have the advantages of a high theoretical electrical capacity (820 mAh g^{-1}), a low redox potential (0.76 V compared to standard hydrogen electrodes), abundant resources, and low prices [8]. High-performance cathode materials such as B/N co-doped porous carbon [9], carbon nanotubes (CNT) [10,11], graphene (GO) [12], and commercial activated carbon (AC) [13,14] have been widely studied and applied. However, the development of practical AZHSs requires the consideration of a suitable electrolyte, as a suitable electrolyte can inhibit the dendrite growth of the Zn anode [15], thereby improving the cycling performance of the device. More importantly, the precise matching of the electrolyte ion size to the aperture of the carbon material facilitates its fast insertion/de-insertion inside the cathode, enhancing the energy density and output

power of the device [16]. Therefore, the development of high-performance electrolytes is of great importance for the popularization of AZHSs.

In terms of electrolyte development, the high safety, relaxed preparation conditions, and low cost have been the eye-catching advantages of water-based electrolytes [17]. However, the AC cathodes of AZHSs still suffer from low energy density and the surface generation of side reactants [18]. Current aqueous electrolytes such as $ZnSO_4$ and $Zn(CF_3SO_3)_2$ are not able to provide the ideal energy density for AZHSs [19], nor can they solve the problem of the precipitation of side reactants on the surface of the cathode material [20]. Therefore, it is necessary to prepare a high energy density or inhibit the side reactants of high-performance aqueous electrolytes for AZHSs using new strategies. At present, many researchers consider the development of hybrid electrolytes, based on the synergistic effects between the ions and ions and between the ions and groups, an effective strategy to enhance the electrochemical performance of ZHSs [21,22], which have made significant progress in the development of organic electrolytes [23], hydrogel electrolytes [24], and organic–hydrogel electrolytes [25]. However, applying the concept of the synergistic effect between the ions to the development of high-performance aqueous electrolytes is an extremely interesting research idea. Further, different anions of AZHS electrolytes have different physical adsorption processes inside the AC cathode due to the different sizes and ion adsorption reaction kinetics between the anions, and the mixing of multiple anions is highly likely to have synergistic or antagonistic effects [26] that affect the electrochemical performance of the device. Here, 2 M $ZnSO_4$, 2 M $ZnCl_2$, and 2 M $Zn(CF_3SO_3)_2$ aqueous solutions were used as electrolytes, AC was used as a cathode, and Zn was used as an anode to determine whether a 2 M $ZnSO_4$ electrolyte was suitable as a mother liquor. Subsequently, we focused on the most suitable addition of $ZnCl_2$ and $Zn(CF_3SO_3)_2$ in the 2 M $ZnSO_4$ electrolyte to determine whether there is an interaction between the SO_4^{2-}, Cl^-, and $CF_3SO_3^-$ anions.

We report that this hybrid anionic electrolyte enhanced the specific capacity and rate capability of the AC cathode through the synergistic effect between the SO_4^{2-}, Cl^-, and $CF_3SO_3^-$. Last but not least, this hybrid anionic electrolyte with the coexistence of SO_4^{2-}, Cl^-, and $CF_3SO_3^-$ increased the energy consumption of the AC cathode surface groups for binding H^+, reduced the consumption of H^+ in the electrolyte during the discharge of AZHSs, and made it difficult to form a local alkaline environment on the AC cathode surface, which inhibited the precipitation of $Zn_4SO_4(OH)_6{\cdot}5H_2O$, thus avoiding damage to the precision structure of the device due to the growth of dendrites on the surface of the AC cathode. The experimental results showed that the electrochemical performance of the 2 M $ZnSO_4$ electrolyte was better than those of the 2 M $ZnCl_2$ and 2 M $Zn(CF_3SO_3)_2$ electrolytes. The specific capacities of the assembled AC cathode//2 M $ZnSO_4$(aq)//Zn anode energy storage devices were 115 and 41 mAh g^{-1} at 0.1 and 5 Ag^{-1} current densities, respectively. Due to the synergistic effect between the anions, the 2 M $ZnSO_4$ + 0.01 M $ZnCl_2$, 2 M $ZnSO_4$ + 0.02 M $Zn(CF_3SO_3)_2$, and 2 M $ZnSO_4$ + 0.01 M $Zn(CF_3SO_3)_2$ + 0.01 M $ZnCl_2$ electrolytes had high energy densities of 133, 124, and 136 mAh g^{-1} at a current densities of 0.1 A g^{-1}, respectively. The prepared electrolyte of 2 M $ZnSO_4$ + 0.01 M $Zn(CF_3SO_3)_2$ + 0.02 M $ZnCl_2$ achieved a specific capacity of 69 mAh g^{-1} at a current density of 5 A g^{-1}. Therefore, the concept of anion co-doping opens a new direction for the development of AZHS electrolytes and provides an important reference for the development of hybrid aqueous electrolytes.

2. Methods and Methods

2.1. Preparation of AZHS Electrodes

An AC cathode was prepared by mixing an AC powder, acetylene black, and polyvinylidene fluoride (PVDF) dispersion in a mass ratio of 8:1:1 and then coated on a stainless-steel mesh (the prepared electrodes needed to be dried in an oven at 60 °C for 8 h). The stainless-steel mesh size was 1 cm × 2 cm, and the load capacity was 1 mg cm^{-2} [15]. The thickness of the zinc foil was 0.1 mm. It was purchased from Tianjin Anuohe New Energy Technology

Co., Ltd. in China, polished, and directly used as an anode electrode. The energy storage device with an AC cathode//2 M $ZnSO_4$(aq)//Zn anode system was assembled with a hybrid anionic electrolyte, AC cathode, Zn anode, and electrochemical cell shell [27].

2.2. Formulation of AZHS Electrolytes

Three electrolytes (2 M $ZnSO_4$, 2 M $ZnCl_2$, and 2 M $Zn(CF_3SO_3)_2$) were prepared to evaluate the effect of electrolyte type on the electrochemical performance of AZHSs in order to show the effect of the hybrid anionic electrolyte on the electrochemical performance of AZHSs doped with 0.005 M, 0.01 M, 0.02 M, 0.03 M, and 0.05 M $ZnCl_2$ or $Zn(CF_3SO_3)_2$ electrolyte in the 2 M $ZnSO_4$ electrolyte. Subsequently, $ZnCl_2$ and $Zn(CF_3SO_3)_2$ were co-doped in the 2 M $ZnSO_4$ electrolyte to observe the effects of anion interactions on the electrochemical properties of AZHSs.

2.3. Material Characterization

Field emission scanning electron microscopy (SEM, JSM-7800F, Japan) was used to characterize the morphologies of the Zn anodes and AC cathodes. X-ray diffractograms of Cu Kα irradiation (λ = 1.54178 Å) were recorded with an X-ray diffractometer (XRD, Rigaku Ulitma IV, Japan) to observe the surface material structures of the Zn anodes and AC cathodes. An X-ray photoelectron spectrometer (XPS, Thermo Scientific ESCALAB 250Xi) was used for the elemental analyses of the Zn anode and AC cathode.

2.4. Electrochemical Performance Testing of AZHS Electrodes

AZHSs were tested for electrochemical properties, including the cyclic voltammetry (CV), constant current charge/discharge technique (GCD), electrochemical impedance spectroscopy (EIS), and Tafel curve measurements. The CV and EIS tests were performed on a CHI 660 electrochemical workstation with an AC cathode as the working electrode and Zn as the counter and reference electrodes. GCD tests were performed on a Sunway High Performance Battery Testing System with a voltage range of 0.2–1.8 V, and the specific capacities of AZHSs were evaluated at current densities of 0.1, 1, and 5 A g^{-1}. In order to show that AZHSs are stable, they were charged and discharged for 200 cycles at a current density of 1 A g^{-1}. In order to exclude the effect of the Zn^{2+} concentration on the performance of AZHSs, a hybrid anionic electrolyte with the same Zn^{2+} concentration and a $ZnSO_4$ solution were prepared and charged and discharged for 1000 cycles at a current density of 5 A g^{-1}. Tafel measurements were performed on a CHI 660 electrochemical workstation with a working electrode with an AC cathode, original Zn foil, used Zn anode, counter electrode of Zn, and reference electrode of saturated glycerol. The specific capacity (C, mAh g^{-1}) for the ZHS device was precisely determined through the discharge curve (GD) by the equation below [9]:

$$C = 2I \int Vdt/3.6Vm \quad (1)$$

3. Results and Discussion

3.1. Comparison of the Performances of Different Electrolytes

As shown in Figure 1a, three AZHS energy storage systems were assembled using a Zn anode and an AC cathode with 2 M $ZnSO_4$, 2 M $ZnCl_2$, and 2 M $Zn(CF_3SO_3)_2$ as the electrolytes. As shown in Figure 1b, the 2 M $ZnSO_4$ electrolyte exhibited a slightly larger peak current density and CV curve integration area than the 2 M $Zn(CF_3SO_3)_2$ electrolyte, indicating a better energy storage performance. In addition, the scan curve of the 2 M $ZnCl_2$ electrolyte was abnormal, which may be due to the irreversible etching of the stainless-steel mesh by the $ZnCl_2$ electrolyte, resulting in the inability of AZHSs to store energy properly. To further illustrate the specific capacity and stability of the three AZHSs, we demonstrated the rate capabilities and cycling performances, and the results are shown in Figure 1c–d. The 2 M $ZnSO_4$ electrolyte in Figure 1c exhibited a higher specific capacity of 115 mAh g^{-1} at a current density of 0.1 A g^{-1}, which was higher than that of the 2 M $Zn(CF_3SO_3)_2$

electrolyte, at 89 mAh g^{-1}. The capacitance retention rate of the 2 M $ZnSO_4$ electrolyte with a 0.1–1 A g^{-1} current density change was 61.7%, which was slightly lower than the 64.5% of the 2 M $Zn(CF_3SO_3)_2$ electrolyte. In addition, the electrolyte voltage of the 2 M $ZnCl_2$ was unable reach 1.8 V. The specific capacity of the 2 M $ZnSO_4$ electrolyte in Figure 1d at a current density of 5 A g^{-1} was 41 mAh g^{-1}, which was higher than the 37 mAh g^{-1} of the 2 M $Zn(CF_3SO_3)_2$ electrolyte. The capacitance retention of the 2 M $ZnSO_4$ electrolyte was 98% after 200 cycles of charge and discharge, which is higher than the 96% of the 2 M $Zn(CF_3SO_3)_2$ electrolyte.

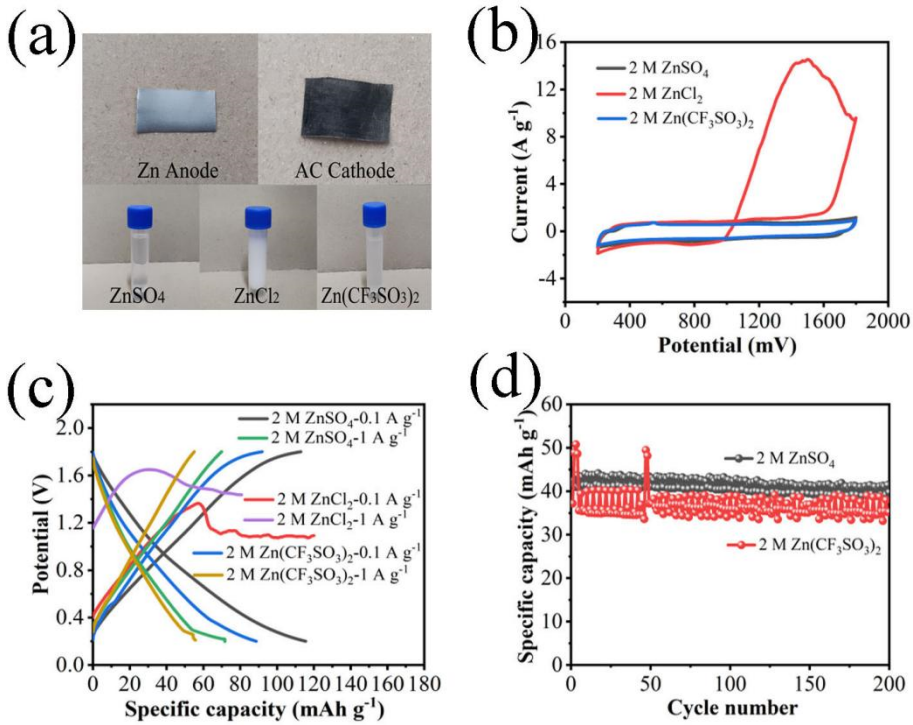

Figure 1. (**a**) Digital photographs of the Zn anode, AC cathode, and 2 M $ZnSO_4$, 2 M $ZnCl_2$, and 2 M $Zn(CF_3SO_3)_2$ electrolytes; (**b**) Comparison of three CV curves (5 mV s^{-1}); (**c**) Rate capabilities of three electrolytes at 0.1 and 1 A g^{-1} current densities; (**d**) Cycling performances (5 A g^{-1}) of 2 M $ZnSO_4$ and 2 M $Zn(CF_3SO_3)_2$ electrolytes.

3.2. Characterization Testing of Zinc Anodes

We observed the electrode states in the AC cathode//2 M $ZnSO_4$(aq) + additive//Zn anode energy storage system by a characterization technique. First, we analyzed the reactions occurring on the zinc anode by electron microscopy scanning (SEM), X-ray diffraction (XRD), and X-ray photoelectron spectroscopy (XPS). The micromorphology and phase analysis results of the zinc foil anode after charging and discharging in different electrolytes are shown in Figure 2. Compared to the pristine zinc foil in Figure 2a, the zinc foil anode after 200 cycles of charging and discharging in the electrolyte exhibited a relatively rough surface (Figure 2b–e). Subsequently, we analyzed the phase composition of the zinc foil anodes with XRD tests. As shown in Figure 2f, the most dominant phase component of the zinc foil anode was always Zn (JCPDS#87-0713), but other diffraction peaks appeared on the surface of the zinc foil anode, which indicated the formation of $Zn_4SO_4(OH)_6{\cdot}5H_2O$ [28] (JCPDS#39-0688) on the surface of the zinc metal. At the same time, the XPS pattern in Figure S1 (see Supplementary Materials) also confirmed the presence of the side reactants.

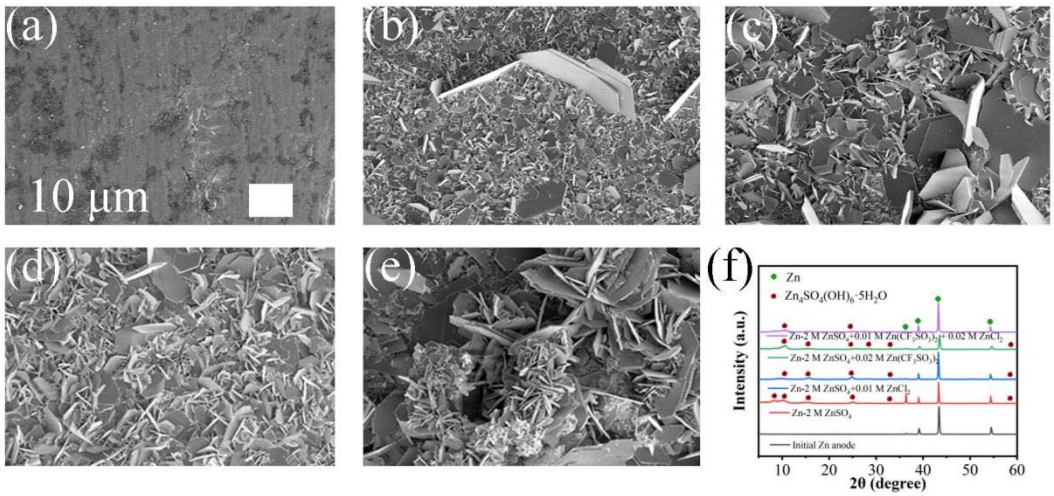

Figure 2. (**a**) Zinc foil; (**b**) Zinc anode in $ZnSO_4$ electrolyte; (**c**) Zinc anode in $ZnSO_4$ + $ZnCl_2$ electrolyte; (**d**) Zinc anode in $ZnSO_4$ + $Zn(CF_3SO_3)_2$ electrolyte; (**e**) Zinc anode in $ZnSO_4$ + $Zn(CF_3SO_3)_2$ + $ZnCl_2$ electrolyte; (**f**) XRD patterns of five zinc anodes.

3.3. AC Characterization Test of AC Cathode

The AZHSs were disassembled, and the AC cathodes were removed, cleaned using pure water for 2–3 min, and dried under vacuum at a temperature of 60 °C for 6 h before a series of characterization tests were performed. From the SEM image in Figure 3a, it can be observed that the AC particles were irregular, the surface was relatively rough, and most of the particles were 5–10 μm in diameter. Due to the faster ion insertion reaction kinetics of H^+, it preferentially undergoes coordination/decoordination reactions with AC cathode surface groups, resulting in Zn^{2+} reacting with OH^- to form $Zn_4SO_4(OH)_6 \cdot 5H_2O$ [29]. The continuous accumulation of these side reactants led to the formation of the lamellar dendrites on the surface of the AC cathode in Figure 3b–d. Compared with Figure 3b–d, we found that the morphology of the AC cathode in the 2 M $ZnSO_4$ + 0.02 M $Zn(CF_3SO_3)_2$ + 0.02 M $ZnCl_2$ electrolyte in Figure 3e was not significantly changed. As shown in the XRD pattern of Figure 3f, the intensity of the AC cathode impurity peaks in the 2 M $ZnSO_4$ + 0.02 M $Zn(CF_3SO_3)_2$ + 0.02 M $ZnCl_2$ electrolyte was significantly weaker than that of the other electrolytes, which once again proved that the electrolyte can effectively inhibit the precipitation of side reactants. The following equation has been reported for the deposition reaction process of $Zn_4SO_4(OH)_6 \cdot 5H_2O$ [15,30]:

$$\{AC\} \ldots \ldots O + H^+ + e^- \rightarrow \{AC\} \ldots \ldots OH \text{ (discharge process)} \quad (2)$$

$$\{AC\} \ldots \ldots OH \rightarrow \{AC\} \ldots \ldots O + H^+ + e^- \text{ (charge process)} \quad (3)$$

$$4Zn^{2+} + 6OH^- + SO_4{}^{2-} + xH_2O = Zn_4SO_4(OH)_6 \cdot xH_2O\downarrow \quad (4)$$

The above equation shows that the binding of the AC cathode surface groups with H^+ is the main reason for the precipitation of $Zn_4SO_4(OH)_6 \cdot 5H_2O$. To investigate the effect of the electrolyte on the occurrence of coordination/non-coordination reactions between the AC cathode surface groups and H^+, we tested the surface overpotential using Tafel curves to determine the ease of electron transfer of the AC cathode surface groups. As shown in Figure 3g,h, the 2 M $ZnSO_4$ + 0.02 M $Zn(CF_3SO_3)_2$ + 0.02 M $ZnCl_2$ electrolyte (1) increased the energy consumption of the H^+ release from the AC cathode surface groups in the charging state, making it difficult to release H^+ and (2) increased the combined energy consumption of H^+ with the AC cathode surface groups in the discharging state, making it difficult to form a local alkaline environment on the AC cathode surface and inhibiting the precipitation of dendrites.

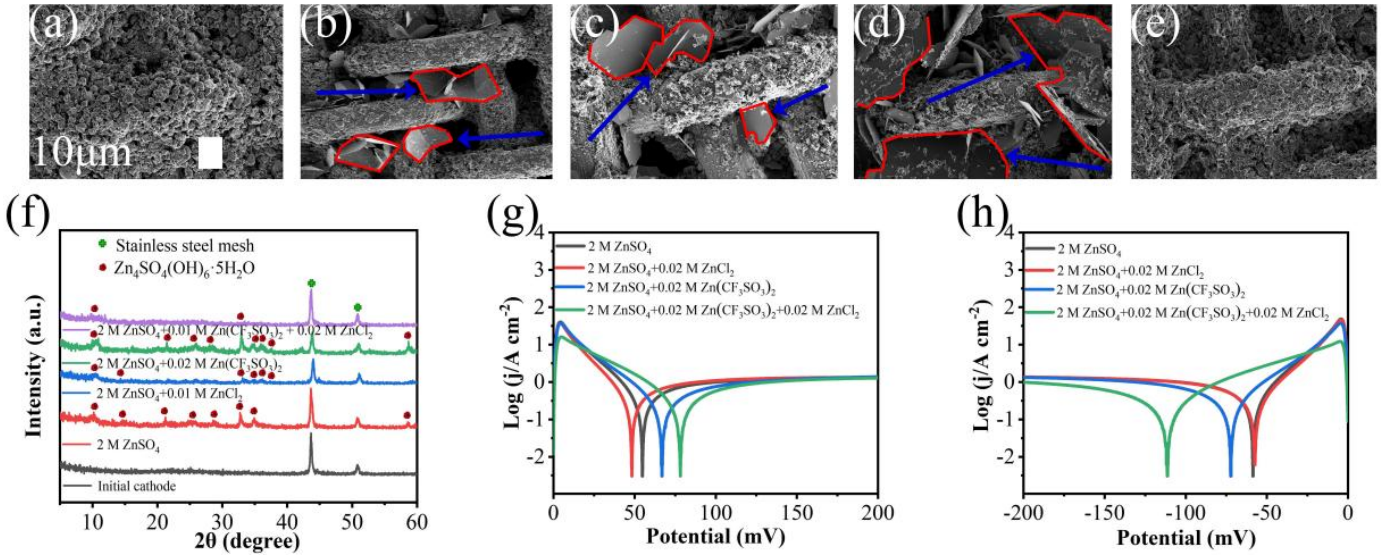

Figure 3. (**a**) AC cathode; (**b**) AC cathode in $ZnSO_4$ electrolyte; (**c**) AC cathode in $ZnSO_4$ + $ZnCl_2$ electrolyte; (**d**) AC cathode in $ZnSO_4$ + $Zn(CF_3SO_3)_2$ electrolyte; (**e**) AC cathode in $ZnSO_4$ + $Zn(CF_3SO_3)_2$ + $ZnCl_2$ electrolyte; (**f**) XRD patterns of 5 AC cathodes; (**g**) AC cathode charge state overpotential; (**h**) AC cathode discharge state overpotential.

3.4. The 2 M $ZnSO_4$ Electrolyte Doped with $ZnCl_2$

First, we tested the electrochemical performance of the 2 M $ZnSO_4$ electrolyte doped with $ZnCl_2$. Figure 4a compares the CV curves of five hybrid anionic electrolytes, which showed approximately rectangular curves, which is a typical electric double-layer energy storage feature. Numbers 1, 2, 3, 4, and 5 of Figure 4b correspond to the 2 M $ZnSO_4$ + 0.005 M $ZnCl_2$, 2 M $ZnSO_4$ + 0.01 M $ZnCl_2$, 2 M $ZnSO_4$ + 0.02 M $ZnCl_2$, 2 M $ZnSO_4$ + 0.03 M $ZnCl_2$, and 2 M $ZnSO_4$ + 0.05 M $ZnCl_2$ electrolytes, respectively. The data show that the electrochemical performance of the 2 M $ZnSO_4$ + 0.01 M $ZnCl_2$ electrolyte was excellent, and the specific capacities at current densities of 0.1, 1, and 5 A g^{-1} were 134, 80, and 59 mAh g^{-1}, which were 16.5, 12.7, and 43.9% higher than those of the 2 M $ZnSO_4$ electrolyte, respectively. The cyclic test in Figure 4c showed that the 2 M $ZnSO_4$ + 0.01 M $ZnCl_2$ electrolyte had good cyclic stability, with a capacitance retention of 97% after 200 cycles at a current density of 1 A g^{-1}. To further clarify that the electrochemical performance enhancement of AZHSs was mainly affected by mixed anions, we performed 1000 charge–discharge cycles for the 2 M $ZnSO_4$ + 0.01 M $ZnCl_2$ and 2.01 M $ZnSO_4$ electrolytes. The specific capacity of the 2 M $ZnSO_4$ + 0.01 M $ZnCl_2$ electrolyte in Figure 4d was 1.44 times higher than that of the 2.01 M $ZnSO_4$ electrolyte. The capacitance retention of the 2 M $ZnSO_4$ + 0.01 M $ZnCl_2$ electrolyte was 97.4%, which was higher than that of the 2.01 M $ZnSO_4$ electrolyte, at 94.1%. Electrochemical impedance spectroscopy (EIS) is used to further investigate the electron/ion transport properties inside the electrolyte. Figure 4e shows the Nyquist curves in the high-frequency region, with the first intercept of the Nyquist curve along the real axis being the electrolyte resistance (Re). It can be seen that with the continuous addition of $ZnCl_2$, the Re values of the 2 M $ZnSO_4$ electrolyte were 9.5, 8.8, 7.8, 7.2, 7.5, and 7.5 Ω. The observed decrease in Re values may be due to the synergistic effect between the SO_4^{2-} and Cl^-, which reduced the internal resistance and improved the conductivity, which in turn increased the specific capacity of AZHSs at a current density of 0.1 A g^{-1} [31]. Figure 4f shows the Nyquist curves in the frequency range of 0.01 Hz–1000 KHz. The data indicate that the synergistic effect of SO_4^{2-} and Cl^- can significantly reduce the equivalent series resistance (ESR) values. However, with the continuous addition of $ZnCl_2$, the electrolyte showed a regular trend of continuous increases in ESR values and a continuous decrease in the surface ion diffusion rate.

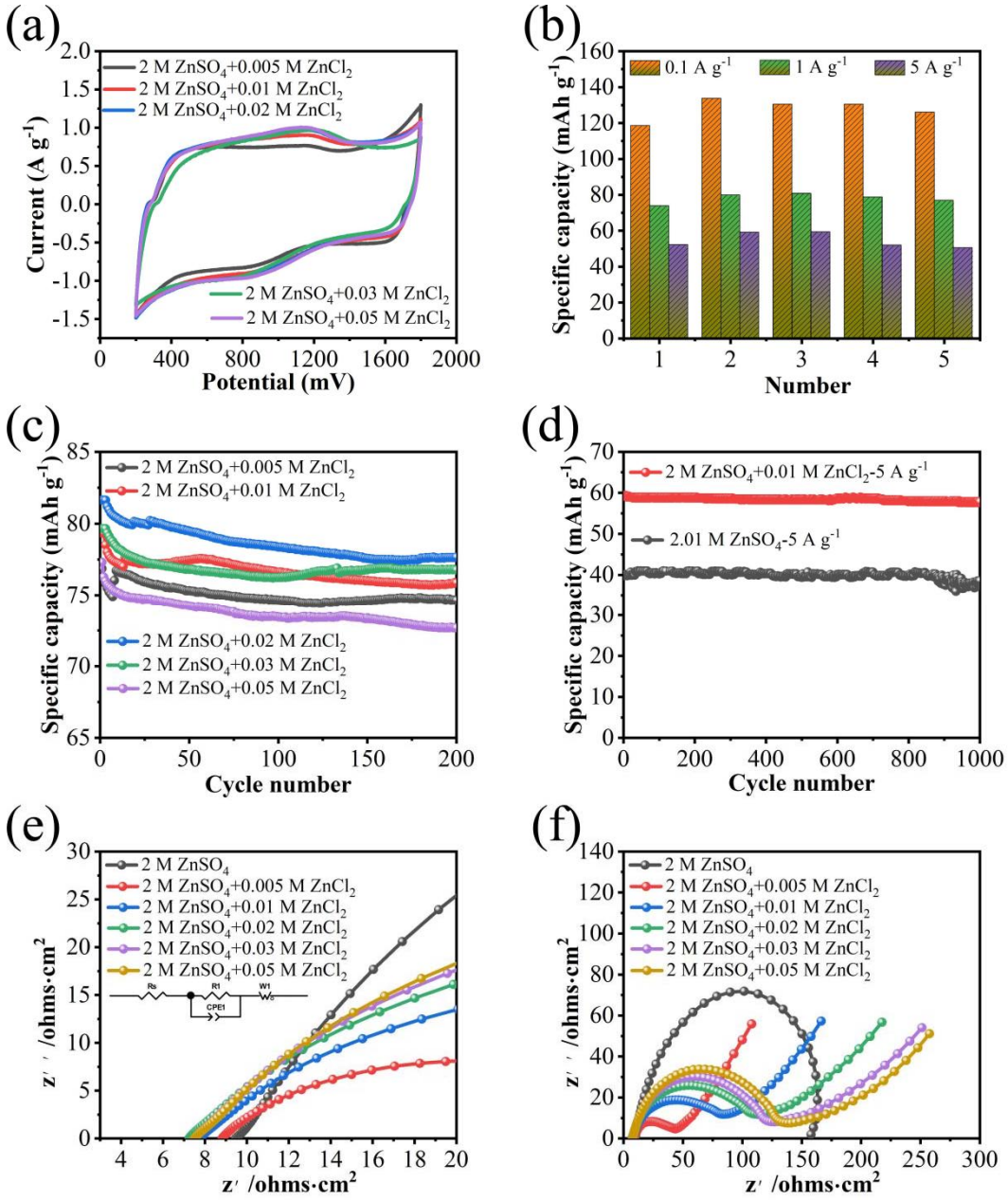

Figure 4. (**a**) Comparison of five CV curves (5 mV s^{-1}); (**b**) Numbers 1, 2, 3, 4, and 5 are 2 M $ZnSO_4$ + 0.005 M $ZnCl_2$, 2 M $ZnSO_4$ + 0.01 M $ZnCl_2$, 2 M $ZnSO_4$ + 0.02 M $ZnCl_2$, 2 M $ZnSO_4$ + 0.03 M $ZnCl_2$, and 2 M $ZnSO_4$ + 0.05 M $ZnCl_2$ electrolytes, respectively; (**c**) Cycling performance (1 A g^{-1}) of hybrid anionic electrolytes; (**d**) Cycling performance (5 A g^{-1}) of electrolytes with the same Zn^{2+} concentration; (**e**) Nyquist plot of hybrid anionic electrolyte in high-frequency region; (**f**) Nyquist plot of hybrid anionic electrolyte.

3.5. The 2 M $ZnSO_4$ Electrolyte Doped with $Zn(CF_3SO_3)_2$

Next, we tested the electrochemical performance of the 2 M $ZnSO_4$ electrolyte doped with $Zn(CF_3SO_3)_2$. Figure 5a compares the CV curves of five hybrid anionic electrolytes, which showed approximately rectangular curves, which is a typical electric double-layer energy storage feature. Numbers 1, 2, 3, 4, and 5 of Figure 5b correspond to the 2 M $ZnSO_4$ + 0.005 M $Zn(CF_3SO_3)_2$, 2 M $ZnSO_4$ + 0.01 M $Zn(CF_3SO_3)_2$, 2 M $ZnSO_4$ + 0.02 M $Zn(CF_3SO_3)_2$, 2 M $ZnSO_4$ + 0.03 M $Zn(CF_3SO_3)_2$, and 2 M $ZnSO_4$ + 0.05 M $Zn(CF_3SO_3)_2$ electrolytes, respectively. The data show that the electrochemical performance of the 2 M $ZnSO_4$ + 0.02 M $Zn(CF_3SO_3)_2$ electrolyte was excellent, and the specific capacities at current densities of

0.1, 1, and 5 A g^{-1} were 134, 80, and 59 mAh g^{-1}, which were 7.8, 23.9, and 63.4% higher than those of the 2 M $ZnSO_4$ electrolyte, respectively. The cycling test in Figure 5c showed that the 2 M $ZnSO_4$ + 0.02 M $Zn(CF_3SO_3)_2$ electrolyte had good cycling stability, with a capacitance retention of 93.4% after 200 charge–discharge cycles at a current density of 1 A g^{-1}. To further clarify that the specific capacity enhancement of AZHSs was mainly influenced by the mixed anions, we performed 1000 charge–discharge cycles for the 2 M $ZnSO_4$ + 0.02 M $Zn(CF_3SO_3)_2$ and 2.02 M $ZnSO_4$ electrolytes. As shown in Figure 5d, the specific capacity of the 2 M $ZnSO_4$ + 0.02 M $Zn(CF_3SO_3)_2$ electrolyte was 1.56 times higher than that of the 2.02 M $ZnSO_4$ electrolyte. The capacitance retention of the 2 M $ZnSO_4$ + 0.02 M $Zn(CF_3SO_3)_2$ electrolyte was 99.5%, which was higher than that of the 2.02 M $ZnSO_4$ electrolyte at 95.1%. Figure 5e shows the Nyquist curves in the high-frequency region. It can be seen that, with the continuous addition of $Zn(CF_3SO_3)_2$, the Re values of the 2 M $ZnSO_4$ electrolyte were 9.5, 10.5, 11.5, 13.6, 11.8, and 12.2 Ω, respectively. The observed increase in the Re value may be attributed to the larger resistance value of $Zn(CF_3SO_3)_2$ (Figure S2 please see the supplementary materials). Figure 5f shows the Nyquist curves in the frequency range of 0.01 Hz–1000 KHz. The data suggest that the synergistic effect of SO_4^{2-} and $CF_3SO_3^-$ can significantly reduce the equivalent series resistance (ESR) values. With the continuous addition of $Zn(CF_3SO_3)_2$, the electrolyte showed an irregular trend of ESR value changes and continuous decreases in the surface ion diffusion rate.

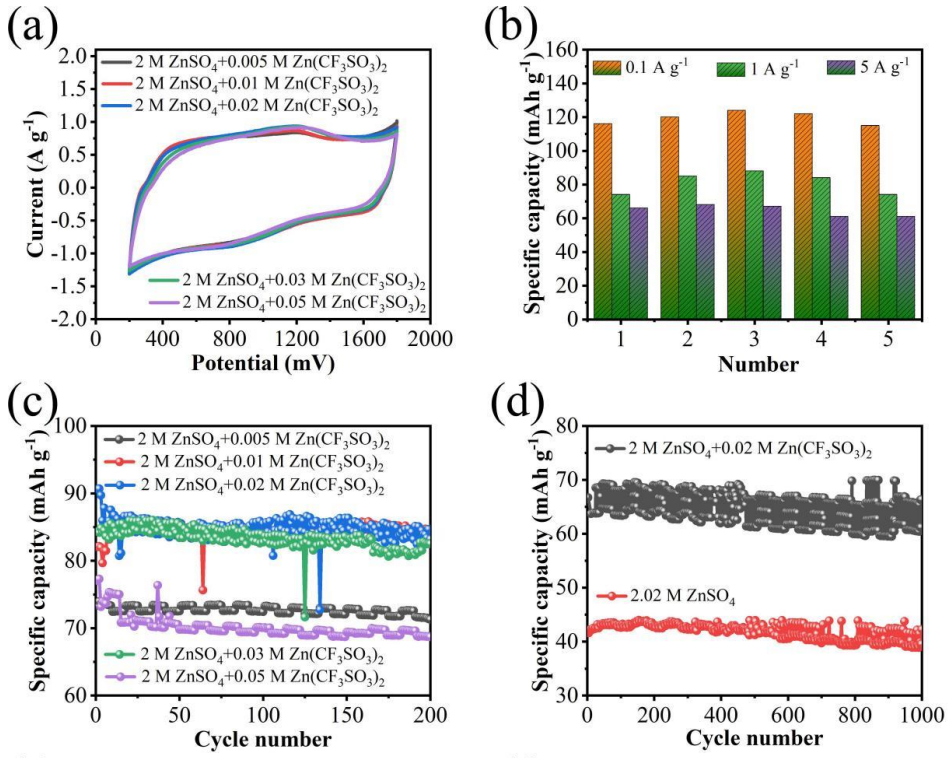

Figure 5. *Cont.*

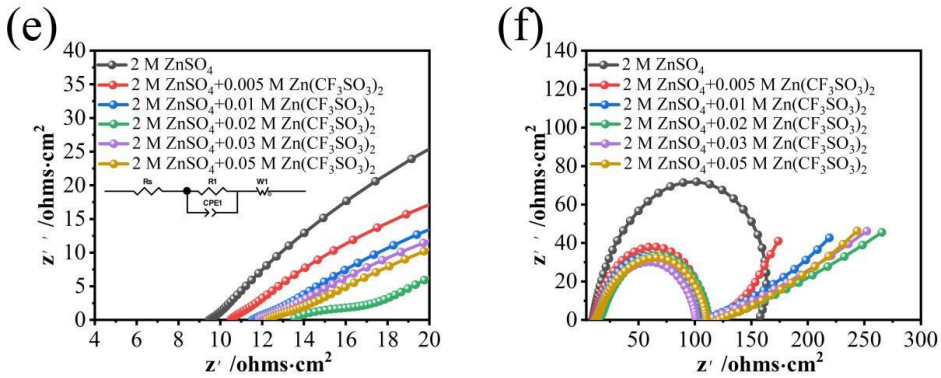

Figure 5. (**a**) Comparison of five CV curves (5 mV s^{-1}); (**b**) Numbers 1, 2, 3, 4, and 5 are 2 M $ZnSO_4$ + 0.005 M $Zn(CF_3SO_3)_2$, 2 M $ZnSO_4$ + 0.01 M $Zn(CF_3SO_3)_2$, 2 M $ZnSO_4$ + 0.02 M $Zn(CF_3SO_3)_2$, 2 M $ZnSO_4$ + 0.03 M $Zn(CF_3SO_3)_2$, and 2 M $ZnSO_4$ + 0.05 M $Zn(CF_3SO_3)_2$ electrolytes, respectively; (**c**) Cycling performance (1 A g^{-1}) of hybrid anionic electrolyte; (**d**) Cycling performance (5 A g^{-1}) of electrolyte with the same Zn^{2+} concentration; (**e**) Nyquist plot of hybrid anionic electrolyte in high-frequency region; (**f**) Nyquist plot of hybrid anionic electrolyte.

3.6. The 2 M $ZnSO_4$ Electrolyte co-Doped with $ZnCl_2$ and $Zn(CF_3SO_3)_2$

Finally, $Zn(CF_3SO_3)_2$ and $ZnCl_2$ were co-doped into a 2 M $ZnSO_4$ electrolyte and subsequently subjected to a series of electrochemical performance tests. Figure 6a compares the CV curves of five hybrid anionic electrolytes, which showed approximately rectangular curves, which is a typical electric double-layer energy storage feature. Numbers 1, 2, 3, 4, and 5 of Figure 6b correspond to the 2 M $ZnSO_4$ + 0.01 M $Zn(CF_3SO_3)_2$ + 0.005 M $ZnCl_2$, 2 M $ZnSO_4$ + 0.01 M $Zn(CF_3SO_3)_2$ + 0.01 M $ZnCl_2$, 2 M $ZnSO_4$ + 0.01 M $Zn(CF_3SO_3)_2$ + 0.02 M $ZnCl_2$, 2 M $ZnSO_4$ + 0.01 M $Zn(CF_3SO_3)_2$ + 0.02 M $ZnCl_2$, 2 M $ZnSO_4$ + 0.02 M $Zn(CF_3SO_3)_2$ + 0.01 M $ZnCl_2$, and 2 M $ZnSO_4$ + 0.03 M $Zn(CF_3SO_3)_2$ + 0.01 M $ZnCl_2$ electrolytes. The data show that the highest specific capacity at a current density of 0.1 A g^{-1} belonged to the 2 M $ZnSO_4$ + 0.01 M $Zn(CF_3SO_3)_2$ + 0.01 M $ZnCl_2$ electrolyte, with a specific capacity of 136 mAh g^{-1}, which was 18.3% higher than that of the 2 M $ZnSO_4$ electrolyte. The highest specific capacity at a current density of 1 A g^{-1} belonged to the 2 M $ZnSO_4$ + 0.01 M $Zn(CF_3SO_3)_2$ + 0.005 M $ZnCl_2$ electrolyte, with a specific capacity of 89 mAh g^{-1}, which was 25.4% higher than that of the 2 M Zn SO_4 electrolyte. The highest specific capacity at a current density of 5 A g^{-1} belonged to the 2 M $ZnSO_4$ + 0.01 M $Zn(CF_3SO_3)_2$ + 0.02 M $ZnCl_2$ electrolyte, with a specific capacity of 69 mAh g^{-1}, which was 68.3% higher than that of the 2 M $ZnSO_4$ electrolyte. The cycling test in Figure 6c showed that the 2 M $ZnSO_4$ + 0.01 M $Zn(CF_3SO_3)_2$ + 0.005 M $ZnCl_2$ electrolyte had good cycling stability, with a capacitance retention of 96.8% after 200 cycles at a current density of 1 A g^{-1}. To further clarify that the capacity enhancement of AZHSs was mainly influenced by the mixed anions, we performed 1000 charge–discharge cycles for the 2 M $ZnSO_4$ + 0.01 M $Zn(CF_3SO_3)_2$ + 0.02 M $ZnCl_2$ and 2.03 M $ZnSO_4$ electrolytes. As shown in Figure 6d, the specific capacity of the 2 M $ZnSO_4$ + 0.01 M $Zn(CF_3SO_3)_2$ + 0.02 M $ZnCl_2$ electrolyte was 1.56 times higher than that of the 2.03 M $ZnSO_4$ electrolyte. The capacitance retention of the 2 M $ZnSO_4$ + 0.01 M $Zn(CF_3SO_3)_2$ + 0.02 M $ZnCl_2$ electrolyte was 99.1%, which was higher than that of the 2.03 M $ZnSO_4$ electrolyte (87.3%). Figure 6e shows the Nyquist curves in the high-frequency region. It can be seen that the co-doping of $Zn(CF_3SO_3)_2$ and $ZnCl_2$ led to an increase in the Re values of the 2 M $ZnSO_4$ electrolyte, with Re values of 9.5, 10.8, 12.2, 9.9, 10.4, and 13.3 Ω. Figure 6f shows the Nyquist curves in the frequency range of 0.01 Hz–1000 KHz. The data suggest that the co-doping of $Zn(CF_3SO_3)_2$ and $ZnCl_2$ gave rise to the complex electron/ion transport properties of the 2 M $ZnSO_4$ electrolyte, as evidenced by the extreme instability of the charge transfer/interface resistance and surface ion diffusion rate. In summary, we have reason to believe that there is a complex electrochemical synergistic process between the SO_4^{2-}, Cl^-, and $CF_3SO_3^-$ in the hybrid

anionic electrolyte that can improve the electrochemical performance of AZHSs and inhibit the dendritic growth of the AC cathode.

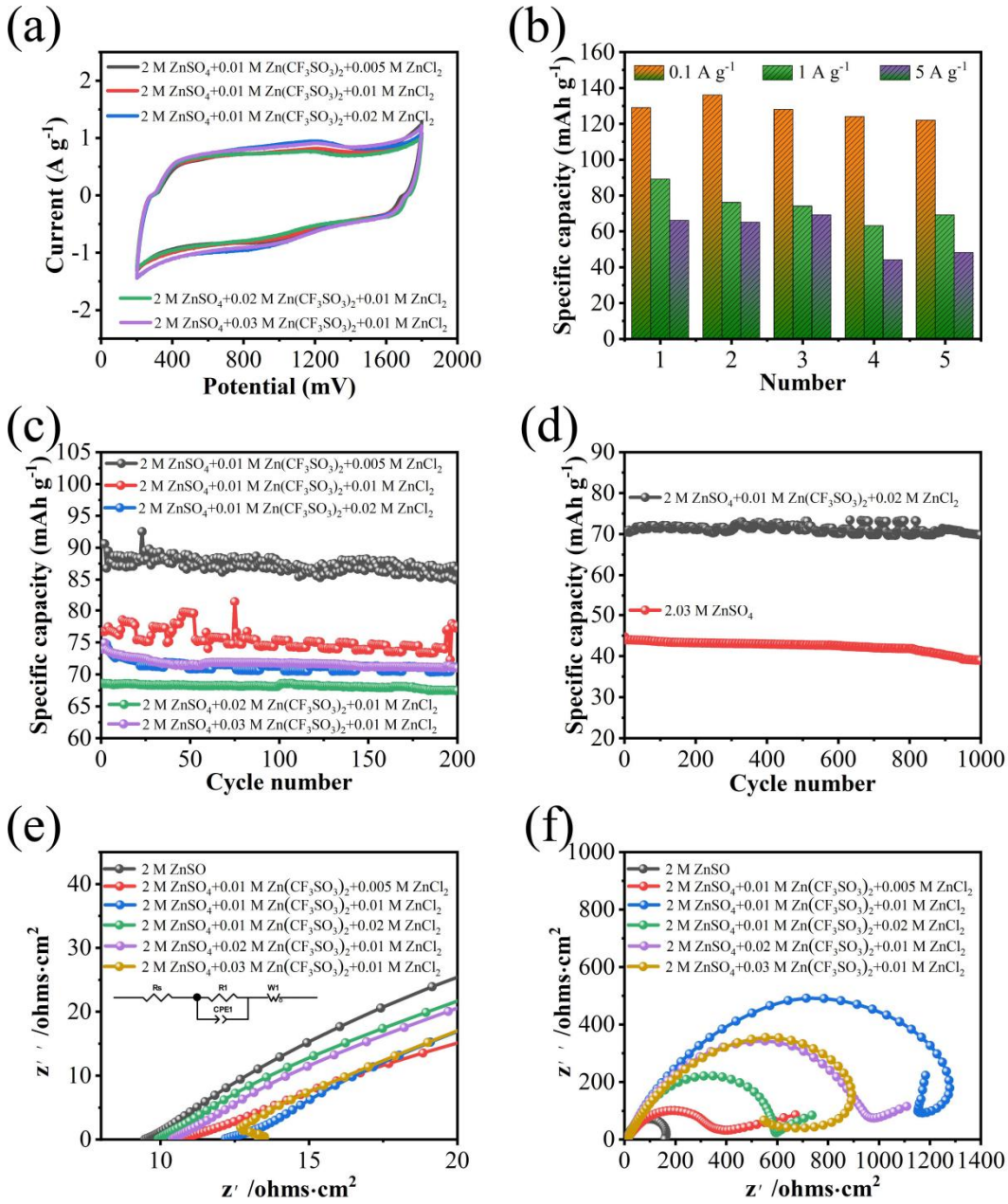

Figure 6. (**a**) Comparison of five CV curves (5 mV s^{-1}); (**b**) Numbers 1, 2, 3, 4, and 5 are 2 M $ZnSO_4$ + 0.01 M $Zn(CF_3SO_3)_2$ + 0.005 M $ZnCl_2$, 2 M $ZnSO_4$ + 0.01 M $Zn(CF_3SO_3)_2$ + 0.01 M $ZnCl_2$, 2 M $ZnSO_4$ + 0.01 M $Zn(CF_3SO_3)_2$ + 0.02 M $ZnCl_2$, 2 M $ZnSO_4$ + 0.02 M $Zn(CF_3SO_3)_2$ + 0.01 M $ZnCl_2$, and 2 M $ZnSO_4$ + 0.03 M $Zn(CF_3SO_3)_2$ + 0.01 M $ZnCl_2$ electrolytes; (**c**) Cycling performance (1 A g^{-1}) of hybrid anionic electrolyte; (**d**) Cycling performance (5 A g^{-1}) of electrolyte with the same Zn^{2+} concentration; (**e**) Nyquist plot of hybrid anionic electrolyte in high-frequency region; (**f**) Nyquist plot of hybrid anionic electrolyte.

4. Conclusions

The performance of AZHSs is limited by the electrochemical properties of the electrolyte. It is necessary to prepare high energy density or inhibit the side reactants of high-performance aqueous electrolytes for AZHSs. We report an aqueous hybrid anionic electrolyte based on $ZnSO_4$, $ZnCl_2$, and $Zn(CF_3SO_3)_2$ and demonstrate that there is a syn-

ergistic effect between the SO_4^{2-}, Cl^-, and $CF_3SO_3^-$ that can significantly enhance the electrochemical performance of AZHSs. In addition, we found that the coexistence of SO_4^{2-}, Cl^-, and $CF_3SO_3^-$ in the electrolytes of AZHSs can effectively inhibit the precipitation of $Zn_4SO_4(OH)_6{\cdot}5H_2O$ by increasing the coordination/uncoordinated energy consumption of AC surface groups with H^+. The results show that the specific capacities of the AC cathode//2 M $ZnSO_4$(aq)//Zn anode energy storage system were 115 and 41 mAh g^{-1} at 0.1 and 5 A g^{-1} current densities. The specific capacity at the 0.1 Ag^{-1} current density was enhanced to 136 mAh g^{-1} by doping 0.5% $ZnCl_2$ and 0.5% $Zn(CF_3SO_3)_2$ in the 2 M $ZnSO_4$ electrolyte. The specific capacity at the 5 Ag^{-1} current density was enhanced to 69 mAh g^{-1} by doping 1% $ZnCl_2$ and 0.5% $Zn(CF_3SO_3)_2$ in the 2 M $ZnSO_4$ electrolyte. More importantly, this concept of anionic co-doping will guide the further development of the most suitable electrolytes for AZHSs.

Supplementary Materials: The following supporting information can be downloaded at: https://www.mdpi.com/article/10.3390/en16010248/s1, Figure S1; Figure S2.

Author Contributions: Conceptualization, B.X. and J.H.; methodology, B.X. and S.L.; writing—original draft preparation, B.X. and Y.S.; writing—review and editing, J.H. and J.L.; funding acquisition, J.L. All authors have read and agreed to the published version of the manuscript.

Funding: The authors acknowledge the financial support from the National Natural Science Foundation of China (12064050); the key R&D Plan of Yunnan Province (202203AC100004); the Major Project of Science and Technology of Yunnan Province (202002AE090010); and the Scientific Research Fund of the Yunnan Provincial Department of Education (2022Y291).

Institutional Review Board Statement: Not applicable.

Informed Consent Statement: Not applicable.

Data Availability Statement: Not applicable.

Conflicts of Interest: The authors declare no conflict of interest.

References

1. Chen, S.G.; Zhang, M.F.; Zou, P.M.; Sun, B.Y.; Tao, S.W. Historical development and novel concepts on electrolytes for aqueous rechargeable batteries. *Energy Environ. Sci.* **2022**, *15*, 1805–1839. [CrossRef]
2. Gao, M.; Wang, W.-K.; Zheng, Y.-M.; Zhao, Q.-B.; Yu, H.-Q. Hierarchically porous biochar for supercapacitor and electrochemical H_2O_2 production. *Chem. Eng. J.* **2020**, *402*, 126171. [CrossRef]
3. Fu, M.; Lv, R.; Lei, Y.; Terrones, M. Ultralight Flexible Electrodes of Nitrogen-Doped Carbon Macrotube Sponges for High-Performance Supercapacitors. *Small* **2021**, *17*, 2004827. [CrossRef] [PubMed]
4. Sun, Q.; Cao, Z.; Wang, S.; Sun, L.; Zhou, L.; Xue, H.; Ming, J. Bio-inspired heteroatom-doped hollow aurilave-like structured carbon for high-performance sodium-ion batteries and supercapacitors. *J. Power Sources* **2020**, *461*, 228128. [CrossRef]
5. Xu, X.L.; Chen, Y.; Zheng, D.; Ruan, P.C.; Cai, Y.H.; Dai, X.J.; Cao, X.H. Ultra-Fast and Scalable Saline Immersion Strategy Enabling Uniform Zn Nucleation and Deposition for High-Performance Zn-Ion Batteries. *Small* **2021**, *17*, e2101901. [CrossRef]
6. Zhang, Q.; Luan, J.Y.; Tang, Y.G.; Ji, X.B.; Wang, H.Y. Interfacial Design of Dendrite-Free Zinc Anodes for Aqueous Zinc-Ion Batteries. *Angew. Chem. Int. Edit.* **2020**, *59*, 13180–13191. [CrossRef]
7. Wang, F.; Borodin, O.; Gao, T.; Fan, X.; Sun, W.; Han, F.; Wang, C. Highly reversible zinc metal anode for aqueous batteries. *Nat. Mater.* **2018**, *17*, 543–549. [CrossRef]
8. Getie, F.A.; Ayele, D.W.; Habtu, N.G.; Yihun, F.A.; Yemata, T.A. Development of electrolytes for rechargeable zinc-air batteries: Current progress, challenges, and future outlooks. *SN Appl. Sci.* **2022**, *4*, 270. [CrossRef]
9. Lu, Y.Y.; Li, Z.W.; Bai, Z.Y.; Mi, H.Y.; Ji, C.C.; Pang, H.; Qiu, J.S. High energy-power Zn-ion hybrid supercapacitors enabled by layered B/N co-doped carbon cathode. *Nano Energy* **2019**, *66*, 104132. [CrossRef]
10. Tian, Y.H.; Amal, R.; Wang, D.W. An Aqueous Metali-ion Capacitor with Oxidized Carbon Nanotubes and Metalicn Zinc Electrodes. *Front. Energy Res.* **2016**, *4*, 34. [CrossRef]
11. Sun, G.; Yang, H.; Zhang, G.; Gao, J.; Jin, X.; Zhao, Y.; Qu, L. A capacity recoverable zinc-ion micro-supercapacitor. *Energy Environ. Sci.* **2018**, *11*, 3367–3374. [CrossRef]
12. Wu, S.L.; Chen, Y.T.; Jiao, T.P.; Zhou, J.; Cheng, J.Y.; Liu, B.; Zhang, W.J. An Aqueous Zn-Ion Hybrid Supercapacitor with High Energy Density and Ultrastability up to 80000 Cycles. *Adv. Energy Mater.* **2019**, *9*, 1902915. [CrossRef]
13. Wang, H.; Wang, M.; Tang, Y. A novel zinc-ion hybrid supercapacitor for long-life and low-cost energy storage applications. *Energy Storage Mater.* **2018**, *13*, 1–7. [CrossRef]

14. Chen, S.; Ma, L.; Zhang, K.; Kamruzzaman, M.; Zhi, C.; Zapien, J.A. A flexible solid-state zinc ion hybrid supercapacitor based on co-polymer derived hollow carbon spheres. *J. Mater. Chem. A* **2019**, *7*, 7784–7790. [CrossRef]
15. Dong, L.B.; Ma, X.P.; Li, Y.; Zhao, L.; Liu, W.B.; Cheng, J.Y.; Kang, F.Y. Extremely safe, high-rate and ultralong-life zinc-ion hybrid supercapacitors. *Energy Storage Mater.* **2018**, *13*, 96–102. [CrossRef]
16. Rashidi, N.A.; Chai, Y.H.; Ismail, I.S.; Othman, M.F.H.; Yusup, S. Biomass as activated carbon precursor and potential in supercapacitor applications. *Biomass Convers. Biorefinery* **2022**, 1–15. [CrossRef]
17. Zhang, T.S.; Tang, Y.; Guo, S.; Cao, X.X.; Pan, A.Q.; Fang, G.Z.; Liang, S.Q. Fundamentals and perspectives in developing zinc-ion battery electrolytes: A comprehensive review. *Energy Environ.* **2020**, *13*, 4625–4665. [CrossRef]
18. Gong, X.; Chen, J.; Lee, P.S. Zinc-Ion Hybrid Supercapacitors: Progress and Future Perspective. *Batter. Supercaps* **2021**, *4*, 1529–1546. [CrossRef]
19. Wan, F.; Zhang, L.L.; Dai, X.; Wang, X.Y.; Niu, Z.Q.; Chen, J. Aqueous rechargeable zinc/sodium vanadate batteries with enhanced performance from simultaneous insertion of dual carriers. *Nat. Commun.* **2018**, *9*, 1656. [CrossRef]
20. Pan, H.L.; Shao, Y.Y.; Yan, P.F.; Cheng, Y.W.; Han, K.S.; Nie, Z.M.; Liu, J. Reversible aqueous zinc/manganese oxide energy storage from conversion reactions. *Nat. Energy* **2016**, *1*, 16039. [CrossRef]
21. Shen, Y.H.; Liu, B.; Liu, X.R.; Liu, J.; Ding, J.; Zhong, C.; Hu, W.B. Water-in-salt electrolyte for safe and high-energy aqueous battery. *Energy Storage Mater.* **2021**, *34*, 461–474. [CrossRef]
22. Wang, G.Q.; Liu, J.Q.; Dong, W.N.; Yan, C.; Zhang, W. Nitrogen/sulfur co-doped porous carbon nanosheets and its electrochemical performance. *Acta Phys. Sin.* **2018**, *67*.
23. Zhang, L.; Liu, Z.; Wang, G.; Feng, J.; Ma, Q. Developing high voltage $Zn(TFSI)_2/Pyr_{14}TFSI/AN$ hybrid electrolyte for a carbon-based Zn-ion hybrid capacitor. *Nanoscale* **2021**, *13*, 17068–17076. [CrossRef] [PubMed]
24. Yang, L.; Song, L.; Feng, Y.; Cao, M.; Zhang, P.; Zhang, X.-F.; Yao, J. Zinc ion trapping in a cellulose hydrogel as a solid electrolyte for a safe and flexible supercapacitor. *J. Mater. Chem.* **2020**, *8*, 12314–12318. [CrossRef]
25. Wang, H.; Li, X.; Jiang, D.; Wu, S.; Yi, W.; Sun, X.; Li, J. Organohydrogel electrolyte-based flexible zinc-ion hybrid supercapacitors with dendrite-free anode, broad temperature adaptability and ultralong cycling life. *J. Power Sources* **2022**, *528*, 231210. [CrossRef]
26. Zhang, Y.J.; Chen, H.L.; Wang, S.J.; Zhao, X.; Kong, F.G. Regulatory pore structure of biomass-based carbon for supercapacitor applications. *Microporous Mesoporous Mater.* **2020**, *297*, 110032. [CrossRef]
27. Nguyen, T.; Tran, T.; Zhao, M.; Geng, S.; Ivey, D.G. Ethylene Glycol as an Antifreeze Additive and Corrosion Inhibitor for Aqueous Zinc-Ion Batteries. *Batter. Supercaps* **2022**, *5*, e202100420.
28. Chen, M.F.; Chen, J.Z.; Zhou, W.J.; Han, X.; Yao, Y.G.; Wong, C.P. Realizing an All-Round Hydrogel Electrolyte toward Environmentally Adaptive Dendrite-Free Aqueous Zn-MnO_2 Batteries. *Adv. Mater.* **2021**, *33*, 2007559. [CrossRef]
29. Tie, Z.W.; Liu, L.J.; Deng, S.Z.; Zhao, D.B.; Niu, Z.Q. Proton Insertion Chemistry of a Zinc-Organic Battery. *Angew. Chem. Int. Edit.* **2020**, *59*, 4920–4924. [CrossRef]
30. Huang, J.H.; Wang, Z.; Hou, M.Y.; Dong, X.L.; Liu, Y.; Wang, Y.G.; Xia, Y.Y. Polyaniline-intercalated manganese dioxide nanolayers as a high-performance cathode material for an aqueous zinc-ion battery. *Nat. Commun.* **2018**, *9*, 2906. [CrossRef]
31. Biesheuvel, P.M.; Bazant, M.Z. Nonlinear dynamics of capacitive charging and desalination by porous electrodes. *Phys. Rev. E* **2010**, *81*, 031502. [CrossRef] [PubMed]